P13.5 POLARIMETRIC RADAR SIGNATURES OF HYDROMETEORS OBSERVED WITHIN MATURE CONVECTIVE STORMS

Darren R. Clabo*[+], Andrew G. Detwiler, and Paul L. Smith
South Dakota School of Mines and Technology, Rapid City, SD USA
[+]Now at University of Wyoming, Laramie, WY

Abstract

This study examines the polarimetric radar signatures of differing hydrometeor types. *In situ* measurements gathered by a suite of probes on an armored T-28 aircraft and radar data from both the prototype dual-polarimetric WSR-88D in Norman, Oklahoma (KOUN) as well as the CSU-CHILL dual-polarimetric radar were obtained from within thunderstorms. Radar volumes co-located with the positions of the aircraft were found and the polarimetric variables from these volumes extracted and compared with hydrometeor images from the T-28 imaging probes. It was found that Z_h, Z_{dr}, and ρ_{hv} show the most promise in distinguishing between hydrometeor classes. These ideas are then further explored in the context of modifications that may be required to a current, computer-based hydrometeor classification algorithm designed to automatically classify hydrometeor types from polarimetric radar data.

1. INTRODUCTION

Polarimetric radar offers many advantages over conventional weather surveillance radar. The reasons to upgrade the current suite of WSR-88Ds to have polarimetric capabilities go far beyond improving remote precipitation estimation and identifying regions of precipitation containing hail. Knowing the polarimetric radar signatures of differing hydrometeor types can help in understanding the dynamics of severe storms (Kumjian and Ryzhkov 2009), estimating latent heat, evaluating weather modification, and initializing hydrometeor types in mesoscale models, among many other things (Straka *et al*. 2000).

A variety of studies have attempted to link differing polarimetric radar signatures to specific hydrometeor types. Seliga and Bringi (1976), taking measurements in England, realized that by calculating new raindrop size distribution parameters from Z_{dr}, much improvement could be made in remote rainfall rate estimation. They also found that polarimetric radar can help in discrimination between hydrometeor types. Hall *et al*. (1984) furthered these ideas by examining the ranges of Z and Z_{dr} for differing hydrometeor types, including wet hail, aggregates, ice particles, and the hydrometeors contained within the melting layer. Bringi *et al*. (1984) studied hail core evolution with polarimetric radar and found hail has distinct Z_{dr} signatures. Bringi *et al*. (1986a) made quailtative comparisons of the polarimetric radar variables Z, Z_{dr}, and *LDR* with *in situ* measurements from the Wyoming King Air aircraft in regions of rain and graupel in the high plains of Colorado. They also found that these observations were supported by their model calculations. Bringi *et al.* (1986b), utilizing the same radar variables, studied the polarimetric radar signatures of hailstones in the high plains of Colorado. Using model hailstone backscattering parameters, they give likely ranges of polarimetric variables for hailstones.

Straka *et al*. (2000), among others, further synthesized these and other studies in the context of hydrometeor type as related to polarimetric radar signatures. The relationships found are expressed as threshold boundaries in a multi-dimensional polarimetric radar space and can be used to develop an algorithm to automatically deduce a bulk hydrometeor type. They also noted that a better understanding of polarimetric radar signatures through observations would help improve these relationships.

This study builds upon the base of knowledge of the polarimetric radar signatures of differing hydrometeor types by utilizing *in situ* microphysics observations from the T-28 aircraft where co-located with polarimetric radar observations. These observations were made with an armored aircraft that could withstand penetrations of mature convective storms. Thus this dataset provides unique *in situ* observations in areas of convective storms not well studied. The purpose of this research is twofold: (1) to compare polarimetric radar measurements and concurrent *in situ* hydrometeor observations made aloft to better understand the polarimetric radar signatures of various hydrometeor types, and (2) to improve upon the current suite of automated hydrometeor classification algorithms.

The organization of the paper is as follows. After the introduction, section 2 discusses the instrumentation used in this study including two different dual-polarimetric radars and the armored storm-penetrating aircraft. Section 3 discusses how the data were collected and how hydrometeor type was deduced for the present study. Section 4 outlines the results of this study. These results are then discussed in the context of current hydrometeor classification algorithms in section 5 and some discrepancies between the results of this study and those of the current literature are examined. Finally, section 6 presents a summary of this paper.

2. INSTRUMENTATION

This study uses two primary types of observation platforms for data collection: dual-polarimetric radar and the armored T-28 research aircraft. Aircraft observations are compared to the concurrent co-located ground-

**Corresponding author address:* Darren Clabo, Dept. of Atmospheric Sciences, University of Wyoming, Laramie, WY; e-mail: dclabo@uwyo.edu.

based polarimetric radar observations to make inferences about hydrometeor type.

2.1 *Polarimetric radar*

Radar data for this study were obtained from two different S-band dual-polarimetric radars: (1) the prototype polarimetric WSR-88D research radar (referred to as KOUN) operated by the National Severe Storms Laboratory (NSSL) in Norman, OK and (2) the transportable CSU-CHILL radar operated by Colorado State University (CSU). The KOUN research and development radar was upgraded to include polarimetric diversity in the spring of 2002 and is fully described in Doviak *et al*. (2002). It simultaneously transmits the vertical and horizontal electromagnetic (EM) waves so that seven radar observables become available. These are radar reflectivity at the horizontal (Z_h) and vertical (Z_v) polarizations, Doppler velocity (V), spectral width (σ_v), differential reflectivity (Z_{dr}), differential phase (Φ_{dp}), and the magnitude of the cross-correlation coefficient (ρ_{hv}) between two copolar components of the radar echo (Ryzhkov *et al*. 2005). The specific differential phase shift, K_{dp}, essentially the range derivative of Φ_{dp}, can also be extracted.

The CSU-CHILL radar utilizes two klystron transmitters that can alternately pulse at one-half the pulse repetition frequency to emit separate H and V EM wave components (Doviak *et al*. 2002). The alternate transmission of the H and V components allows the CSU-CHILL radar to retrieve another polarimetric variable in addition to those listed for the KOUN radar—the linear depolarization ratio (LDR_{hv}). Descriptions of LDR_{hv} and the rest of the polarimetric variables are quite common in the literature (e.g., Doviak and Zrnić 1993; Straka *et al*. 2000, Bringi and Chandrasekar 2001) and thus are omitted here for brevity.

2.2 T-28 aircraft

The T-28 was a storm penetrating armored aircraft operated by the South Dakota School of Mines and Technology until its retirement in 2004. The instrumentation used in these flights included the Stratton Park Engineering Company (SPEC) High Volume Precipitation Spectrometer (HVPS), the Particle Measuring Systems (PMS) Optical Array Probe (OAP) 2D-C and 2D-P models, and a hail spectrometer. These probes, situated under the wings of the T-28, function by illuminating a set area, normal to the path of aircraft travel, with coherent light and detecting a shadow or occlusion of this light as a particle passes through the sensor (Feind 2006). This shadow is recorded as a two dimensional silhouette of the particle in a plane along the flight path. The aircraft also had instrumentation to measure a variety of state variables.

3. Methodology

3.1 Radar data collection

Data from the KOUN radar were taken from 16 May, 23 May, and 4 June 2003. These three days, during the intensive observation period (IOP) of the Joint Polarization Experiment (JPOLE; Ryzhkov *et al*. 2005), were chosen because they involved a variety of radar echo types, the radar echoes were in close proximity to the radar, and (most importantly) they included airspace that was being sampled by the T-28 aircraft while under radar surveillance.

Aircraft locations and timestamps, taken from the GPS unit on the T-28, were used in calculations to relate the aircraft data to a given radar pixel from KOUN. The T-28 aircraft has a large radar cross section (giving strong skin-paint echoes) and thus was easily seen by the radar; it exhibited relatively distinctive polarimetric radar signatures, most notably in the ρ_{hv} fields. To circumvent the problem of corruption of the hydrometeor signatures by the aircraft echoes, and to provide a larger sample size, generally 60 seconds of aircraft data were utilized (typically covering ~6 km of flight path). This path length was centered on the aircraft/radar colocation point in space and time. Thus it was assumed that in the thirty seconds preceding and following colocation the hydrometeor field did not change significantly over the advection region. This larger dataset then contains a hydrometeor field that closely resembles that of the one the T-28 flew through and includes points that were both influenced by the aircraft signature and free of aircraft contamination issues.

According to Straka and Zrnić (1993), of the meteorological constituents, only wet snow produces values of ρ_{hv} less than 0.90 and only a rain/hail mix produces values from 0.90 to 0.95. Other forms of precipitation tend to yield ρ_{hv} values between 0.95 and 1. There were no particles classified as wet snow in this study and the drops/graupel category—akin to rain/hail—here does not produce values less than 0.95. Thus pixels with values of ρ_{hv} less than 0.91 were removed prior to analysis. Time series charts of ρ_{hv} were created and this threshold was found to separate radar data that were potentially influenced by the aircraft from those based solely on the meteorological constituents.

The CSU-CHILL radar was also employed for this study to obtain more co-located aircraft and radar observations including hail. Two datasets were obtained with radar and T-28 flight data from 25 June and 29 June 2000 during the Severe Thunderstorm Electrification Study (STEPS). Data from the CSU-CHILL radar were obtained using the Virtual Chill (VCHILL) program available online from VCHILL website http://www.chill.colostate.edu/w/VCHILL. The VCHILL program outputs PPI images for each of the polarimetric variables collected (Z, V, Z_{dr}, LDR_h, LDR_v, Φ_{dp}, K_{dp}, and ρ_{hv}). Calculations similar to the ones made during the KOUN data extraction were made to locate the approximate elevation of the aircraft relative to the radar. The track (with associated flight time) of the T-28 aircraft could be then overlaid on the appropriate PPI within the VCHILL program to extract the polarimetric variables.

3.2 Aircraft data collection and hydrometeor classification

Aircraft data, including temperature, liquid water concentration (LWC), pressure, and aircraft airspeed as well as the 2D-C probe imagery and information from the hail spectrometer, were matched to the appropriate

radar pixels. For all of the cases, 2D-C probe imagery data were compiled into groups corresponding to individual radar pixels; generally there were 3-7 seconds of aircraft data per radar pixel, depending on the range from the radar and the orientation of the flight path relative to the radar pixel. The individual 2D-C images were classified into distinct hydrometeor classes following the scheme of Feind (2006). Data from the HVPS were used to augment the 2D-C data in regions of hail. Eight different types of hydrometeors were distinguished in this classification process: drops, snow, hail, columns, needles, dendrites, plates, and "holes". The hole images were attributed to water shedding from the probe tips and thus are not a naturally-produced hydrometeor type. Figure 1 gives examples of the classification output from this scheme for various hydrometeor types.

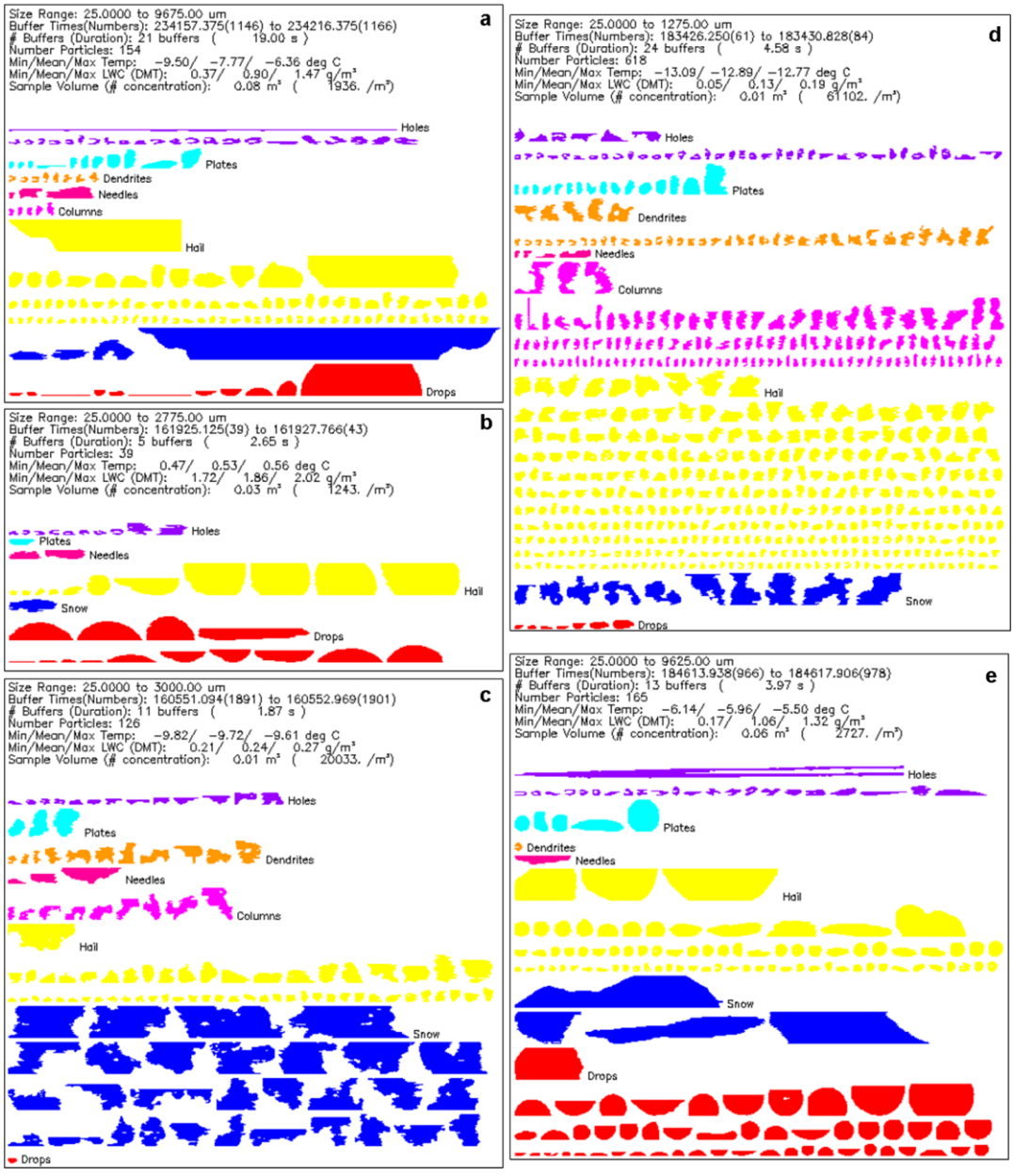

Fig. 1. Example particle images from the 2D-C probe with classifications given by Feind (2006). Note that each image set includes a variety of particle types. Final classifications used in this study are exampled by a) hail, b) drops c) snow, d) graupel, and e) drops/graupel.

These classified images were then further examined by eye to determine the final hydrometeor identification/classification for each group. Based on seven different individual particle classifications produced by the Feind scheme, and subjective evaluation of the particle images, the groups of hydrometeor images corresponding to each radar pixel were assigned to one of five broad hydrometeor categories. These include graupel, snow, drops/graupel, drops, and hail. Descriptions and pictures of these various hydrometeor types are numerous in the literature. Drops (rain and drizzle) are quasi-spherical, with equilibrium shape dependent on size (e.g. Beard and Chuang 1987). Graupel can be subclassified into three different types: hexagonal, conical, and lump, which are all formed via some type of riming (Knight and Knight 1972; Wallace and Hobbs 1977). Snow can be seen in a variety of shapes and sizes from pristine crystals to rimed aggregates (Wallace and Hobbs 1977). Hailstones are built upon a grain of ice, generally have a laminar structure and can be found in various shapes, with or without lobes or protrusions (Knight and Knight 1970; Wallace and Hobbs 1977).

An attempt was made, using values of temperature and LWC, to further sub-divide the snow and graupel classes into wet and dry categories. In this dataset, snow was only observed when the temperature was below zero degrees Celsius—the cutoff used for the wet versus dry snow categories following the criteria found in Straka *et al*. (2000, Table 8). Thus only dry snow is included here. The distinction between wet and dry graupel was a bit more complex, and used both temperature and LWC information. A zero order function was used for discrimination, very loosely based on the table given by Lesins and List (1986, Fig. 11) and fully described by Clabo (2009). The final classification scheme for the *in situ* samples from the 2D-C probe thus includes six categories: drops, drops/graupel, wet graupel, dry graupel, hail, and dry snow.

4. RESULTS

The T-28 storm penetrations were directed for specific purposes in these studies (e.g. to study electric fields, to gather hail data, etc.); the results of this study come from fortuitous data collection. Thus the *in situ* data presented here are inherently non-random samples. For example, the T-28 was directed to avoid any area of a storm where the reflectivity exceeded 55 dBZ—areas too dangerous to sample even with an armored aircraft (though this threshold was on occasion accidentally exceeded). These data also only come from summer-time convective storms over the Great Plains.

Results from this study are presented for both the KOUN and CSU-CHILL data sets. The data that were collected from the CSU-CHILL radar included wet and dry graupel and hail. The KOUN radar observed wet and dry graupel, drops, drops/graupel, and dry snow. Both radars observed wet and dry graupel hydrometeor types; thus these data sets will be consolidated in the data analysis.

There were a total of 1027 seconds of aircraft data included in this study corresponding to nearly 100 km of in-storm flight path. Included are 69 seconds in the wet graupel category, 198 in dry graupel, 507 in dry snow, 27 in drops, 99 in hail, and 127 in drops/graupel. It is obvious that there are a limited number of data points available to analyze, especially in the drops category. But rain is very common, readily detectable in isolation by the radar (e.g. beneath the bright band in areas of stratiform rain), and safely studied by other aircraft, so the focus in this study is given to distinguishing ice and mixed phase hydrometeors.

Figures 2a-d are box and whisker plots showing a few select statistical parameters for the distributions of Z_h, Z_{dr}, ρ_{hv}, and LK_{dp}, respectively, for each of the given hydrometeor types. The whiskers point to the minimum and maximum values and the boxes to the 25th, 50th (median), and 75th percentiles, while the symbol indicates the mean value. For reflectivity in Fig. 2a, the mean Z_h value is highest in the hail category. This would be expected of these larger hydrometeors. The lowest reflectivity values are in the dry snow category. Dry snow has a very low dielectric constant and so, regardless of crystal shape or orientation, it should generally have a lower reflectivity than the other hydrometeors (Straka *et al*. 2000).

Figure 2b presents differential reflectivity, Z_{dr}, for the various hydrometeor types. The highest mean Z_{dr} is seen in the drops category but the observed range is narrow, perhaps due to the limited number of samples. Large drops have a tendency to show, in bulk, positive Z_{dr} values because of their oblate shape with the longest axis parallel to the ground. Smaller drops (~1 mm) exhibit a near-spherical shape, producing Z_{dr} near 0 dB (Beard and Chuang 1987). The drops/graupel category has a mean Z_{dr} somewhat lower than that of the drops category. Both graupel categories fall in the middle of this spectrum for mean Z_{dr}. Although the fall orientation of graupel particles is not well understood (Straka *et al*. 2000), they may rotate or tumble while falling. The tumbling action of these particles would, in bulk, produce a Z_{dr} of ~0 dB and this may be the cause of the lower mean Z_{dr} for these categories. The dry snow category also produces a mean Z_{dr} of near 0 dB. Straka *et al*. (2000) present two schools of thought for the Z_{dr} of snow particles. Pristine dendrites falling primarily horizontally would exhibit a positive Z_{dr}. But snow aggregates and larger dendrites rotate and tumble as they fall and thus show Z_{dr} values closer to 0 dB. Considering that the Feind (2006) classification scheme contains a category for dendrites, and few dendrites were identified using this scheme, the majority of snow particles here are thought to be of tumbling snow aggregates, thus reducing the overall mean Z_{dr}. Hail has the lowest Z_{dr} of any of the categories. It is well known (e.g. Bringi *et al*. 1984; Aydin *et al*. 1986; Balakrishnan and Zrnić 1990) that hail cores produce a local minimum in the Z_{dr} field because hailstones tend to tumble as they fall.

Determining how useful some of this Z_{dr} information is, however, may be difficult. Figure 3 is a plot of Z_h vs. Z_{dr} that shows the differences in observed values of Z_{dr} for graupel for the two radars. These differences are striking and may be not only attributable to environmen-

tal differences in the storms but also to differences in Z_{dr} calibration between the two radars.

Figure 2c is a box and whisker plot of cross-correlation coefficient, ρ_{hv}, for the various hydrometeor types. As previously discussed, this particular variable is very susceptible to the aircraft skin paint but it may also be anomalously low in areas far from the radar due to non-uniform beam filling (NBF), as discussed in Ryzhkov (2007). The mean values of ρ_{hv} are lowest in the hail and wet graupel categories. It is well known that ρ_{hv} tends to decrease in regions of mixed phased hydrometeors (Straka and Zrnić 1993; Straka *et al*. 2000, among others) such as those dominated by wet graupel. As hail falls in bulk, the stones are most likely randomly oriented, thus giving the observed low values of ρ_{hv}. Dry snow has the largest mean value of any of the hydrometeor categories. If the snow is not falling as irregular oriented pristine flakes, it is believed that the ρ_{hv} will be above 0.95 (Straka *et al*. 2000). Because, as stated previously, most of the snow was observed to be dry, low-density aggregates, the returned power of the orthogonal wave components may be well-correlated. Similarly, the drops category should also have a high ρ_{hv}, and though the drops category does have a slightly lower mean ρ_{hv} than dry snow, it is almost 0.99. There are some values of ρ_{hv} greater than one. There is no physical explanation for these values; the likely cause is statistical estimation that would include such things as noise, quantization, and the number of samples (Dusan Zrnić 2009, personal communication).

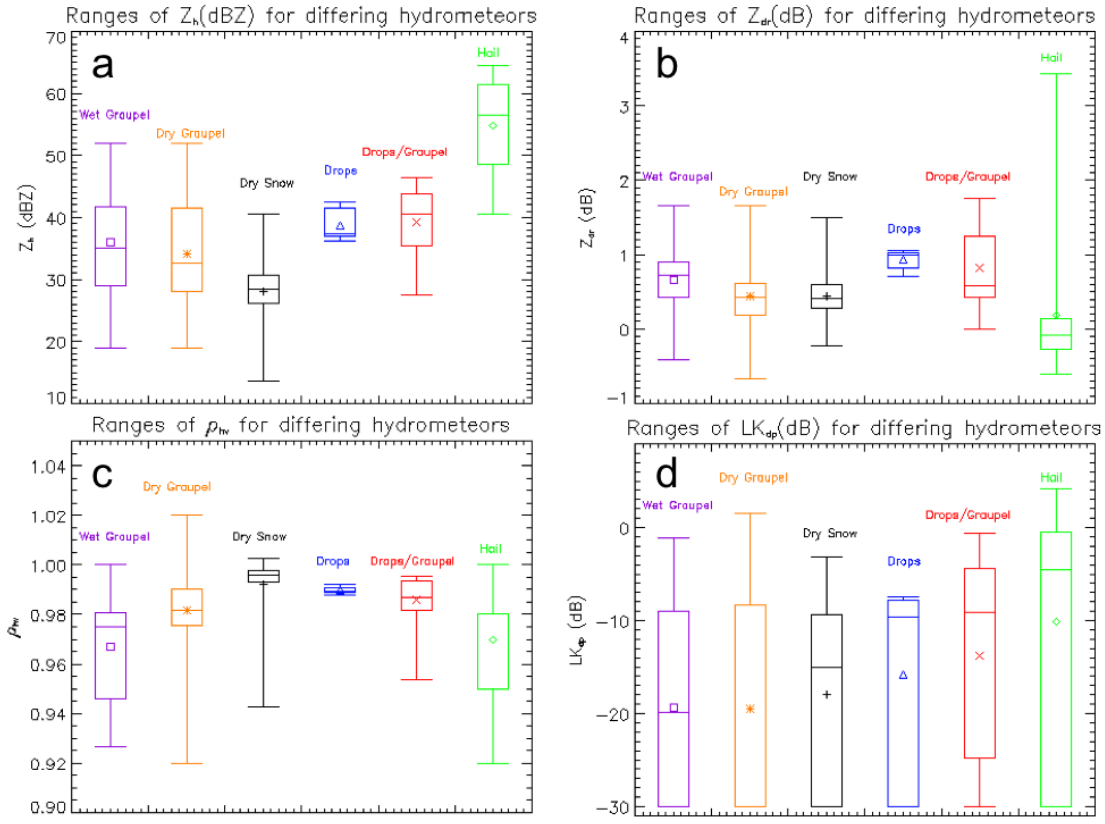

Fig. 2. Box and whisker plots of the differing ranges of data for the five hydrometeor types for (a) Z_h, (b) Z_{DR}, (c) ρ_{hv}, (d) LK_{DP}. The whiskers indicate the minimum and maximum values, the box lines represent the 25th, 50th, and 75th quartiles, and the symbols denote the mean values.

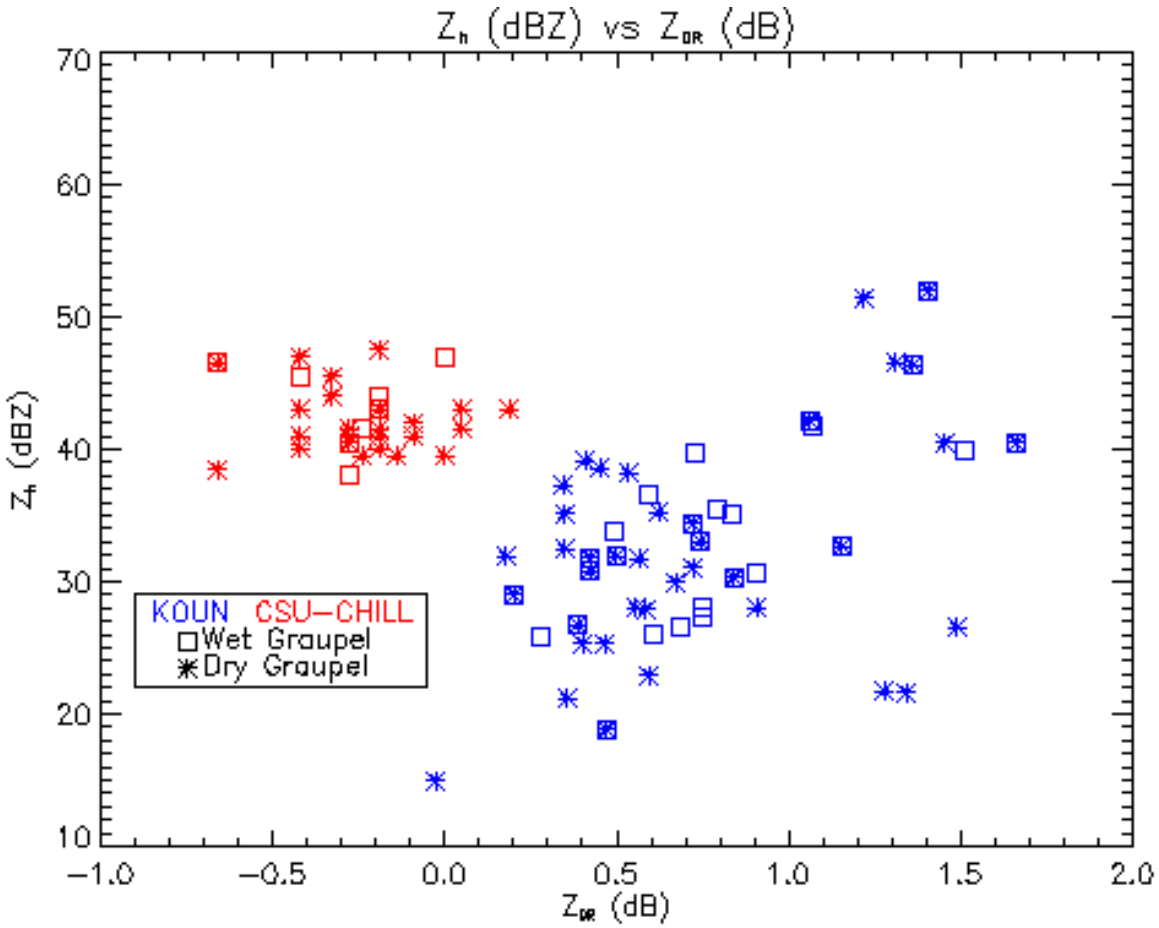

Fig. 3. Plot of Z_h vs Z_{dr} for both the wet (squares) and dry graupel (asterisks) categories showing the differences between the cases observed by the CSU-CHILL (red) and KOUN (blue) radar.

To follow the method used in the hydrometeor classification algorithm of Park *et al*. (2009, herafter P09), K_{dp} is presented in logarithmic form, denoted LK_{dp}, and the statistical parameters for LK_{dp} for the different hydrometeor classes are seen in Figure 2d. Park *et al*. found the logarithm of K_{dp} convenient to use and it has been noted that LK_{dp} is almost linearly dependent on Z_h (in dBZ) for regions of moderate to heavy rain (Alexander Ryzhkov 2009, personal communication). Values for K_{dp} can vary from negative to positive and therefore ranges of values of LK_{dp} pose a problem. For positive K_{dp}, LK_{dp} can range from positive to negative; negative values of K_{dp} have undefined logarithm values so those values (and near-zero positive values) are set to a constant lower limit, in this case -30 dB. Large negative values of K_{dp} (and thus LK_{dp} values set to -30 dB) may be attributed to NBF and may become more frequent as a radar beam widens with greater distance (Ryzhkov 2007). Other negative values of K_{dp} (where LK_{dp} values are also set to -30 dB) may be attributed to ice crystals oriented in bulk vertically—such as those sometimes found in a strong electric field (Ryzhkov and Zrnić 2007). (Currently, the authors are investigating the electric fields from the flight data in the present study to determine if a threshold can be set to remove data influenced by NBF.) These conditions, however, are not manifested in the Z_{dr} fields because Z_{dr}, being reflectivity weighted, is dominated by the larger aggregates that are not as influenced by electric fields. As K_{dp} is not reflectivity weighted, it sees these larger aggregates as relatively symmetrical.

5. IMPLICATIONS FOR HYDROMETEOR CLASSIFICATION ALGORITHMS

Polarimetric radar variables are sensitive to the composition, shape, size, distributions and fall behaviors of hydrometeor scatterers (Liu and Chandrasekar 2000, hereafter LC2000). These variables may also be sensitive to the relative numbers and sizes of the particles within each hydrometeor class. As a result, inferences can often be made concerning the radar-dominant hydrometeor species (and possibly size) that exist within a specific radar volume.

A direct method of classifying the radar-observed hydrometeors can not be employed, though, because differing hydrometeor types do not have mutually exclusive polarimetric radar signatures (Straka and Zrnić 1993). Therefore there may be significant uncertainty in diagnosing a correct classification. However, by using

differing variables combined with some empirical knowledge of hydrometeor characteristics, one can usually arrive at a likely characterization of the dominant bulk hydrometeor type contained within a radar volume.

5.1 Hydrometeor classification algorithms (HCAs)

Considering the large amount of radar data that must be ingested to come to any useful conclusion, an automated procedure must be devised for such classification. Fuzzy-logic classification methods are currently the most commonly employed schemes for hydrometeor classification (LC2000, Zrnić *et al*. 2001, Lim *et al*. 2005, P09, among others). These types of HCAs utilize membership functions that allow for a given value of an input polarimetric variable to belong to a variety of possible hydrometeor categories, each with a different membership function for that variable and a potentially different corresponding "membership degree." Figure 4 shows an example membership function where the ordinate represents the fractional probability that hydrometeors in a radar volume, having the value of the parameter whose range is plotted on the abcissa, might belong to a particular category. A non-symmetrical membership function that is flat on top (maximal value) with ends that taper to a minimum value provides a very good representation.

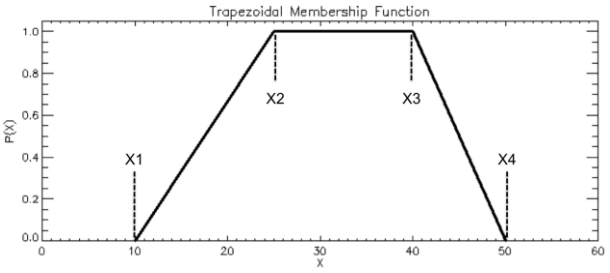

Fig. 4. Illustration of a trapezoidal membership function for an arbitrary polarimetric radar variable X, where X1, X2, X3, and X4 denote the membership function break points.

To create the membership functions, preferred ranges of polarimetric variables for the differing hydrometeor types must be known. Previous studies utilizing *in situ* aircraft measurements (Bringi *et al*. 1986a; Jameson 1987), ground measurements (Bringi *et al*. 1984, Doviak and Zrnić 1993, Ryzhkov *et al*. 2005), and model computations (Seliga and Bringi 1976; Bringi *et al*. 1986b, Balakrishnan and Zrnić 1990; Vivekanandan *et al*. 1990; Doviak and Zrnić 1993) describe the differing hydrometeor types in terms of ranges of the polarimetric variables. The intent of this discussion is to build upon these previous studies by incorporating *in situ* measurements from mature, convective storms, which may be underrepresented in the current literature.

5.2 Implications of the T-28 results

The scheme presented by P09 was recommended by the U.S. National Weather Service to be implemented with the polarimetric upgrades to the current suite of WSR-88Ds. Their study distinguishes between ten different classes of targets: ground clutter/anoma-lous propagation (GC/AP), biological scatterers (BS), dry snow (DS), wet snow (WS), crystals (CR), graupel (GR), big drops (BD), rain (RA), heavy rain (HR), and a rain/hail mixture (RH).

A direct comparison between the hydrometeor classes of the P09 HCA and those of this study is somewhat difficult because of the lack of quantitative descriptions for each hydrometeor type within the P09 HCA discussion. Table 1 shows the classification outputs of several differing HCAs, including P09, along with the classes used in this study. This table was compiled using the different hydrometeor classes from each HCA mentioned, plus the observational study of Feind (2006) and the classifications of the present study. The rows of the table attempt to relate similar hydrometeor types, assuming that the authors of the HCAs define their hydrometeor types in a similar way to that presented in section 3. Though some of the classes have different nomenclature, the similarities between most of the categories suggest that the practical differences between classes may often be negligible and thus intercomparisons can be made.

The HCA of P09 utilizes trapezoidal membership functions for each polarimetric variable for the differing hydrometeor types. Their membership functions are presented in tabular format with four break points, X1, X2, X3, and X4; the four break points correspond to the inflection points illustrated in Fig. 4 (however, it is unclear how they establish these break points). The P09 values for those break points are reproduced here in Tables A1 and A2 in the Appendix. The results of this study are presented in similar form in Table 2. The columns X1, X2, X3, and X4 represent each break point on the trapezoidal membership function as illustrated in Fig. 4. The break point values in the present study were calculated using the minimum value, the 25th percentile, the 75th percentile, and the maximum value for X1, X2, X3, and X4, respectively.

Because of the sampling limitations of the present study, data that fall within the ranges of the membership functions given by P09 are of relatively little further interest. But because many regions of convective storms can only be sampled by an armored aircraft such as the T-28, there may well be an underrepresentation of convective storm data within the current literature. Thus focus here is given to the data that fall outside the polarimetric variable ranges of the membership functions of P09.

Although K_{dp} is presented along with LK_{dp} in Table 2, only the LK_{dp} will be addressed here to parallel the P09 study. Also, discussion of the linear depolarization ratio, LDR_{hv} is limited to the graupel and hail categories observed with the CSU-CHILL radar. Because LDR_{hv} will not be available with the polarimetric WSR-88D radars, discussion of this variable is neglected, though results are still presented in Table 2.

Table 1. Comparisons of hydrometeor classes from current operational HCAs to the classes used in this study.

Zrnić et al. (2001)	Park et al. (2009)	Liu and Chandrasekar (2000)	Feind (2006)	Lim et al. (2005)	Clabo (2009)
		Drizzle	Drops	Drizzle	Drops
Light Rain	Light and Moderate Rain	Rain		Rain	
Moderate Rain					
Heavy Rain	Heavy Rain				
Large Drops	Big Drops				
Rain/Hail	Rain/Hail	Rain/Hail		Small Rain + Hail	Drops/Graupel or Hail
				Large Rain + Hail	
Graupel/Small Hail	Graupel	Dry Graupel	Graupel	Graupel/Small Hail	Dry Graupel
		Wet Graupel			Wet Graupel
Hail		Small Hail	Hail	Small Hail	Hail
		Large Hail		Large Hail	
Dry Snow	Dry Aggre-gated Snow		Snow	Dry Snow	Dry Snow
Wet Snow	Wet Snow			Wet Snow	Wet Snow (none observed)
Horizontal Ice Crystals	Crystals of Different Orientations	Low-Density Ice Crystal	Plates, Columns, Needles		Dry Snow
Vertical Ice Crystals		High Density Ice Crystal			
GC/AP Biological Scatterers (Not in display)	Biological Scatterers				
	Ground Clutter/AP				

Table 2. Observed values for the membership functions found in this study. The points for X1, X2, X3, and X4 are the minimum, 25th percentile, 75th percentile, and maximum values, respectively.

Radar Variable	Hydrometeor Type	X1	X2	X3	X4
Z_h (dBZ)	Wet Graupel	18.83	29.02	41.76	51.95
	Dry Graupel	18.83	27.98	41.50	51.95
	Dry Snow	13.70	26.07	30.68	40.56
	Hail	40.50	48.50	61.50	64.50
	Drops	36.16	36.99	41.56	42.41
	Drops/Graupel	27.51	35.48	43.86	46.52
Z_{dr} (dB)	Wet Graupel	-0.42	0.42	0.90	1.66
	Dry Graupel	-0.66	0.18	0.62	1.66
	Dry Snow	-0.22	0.28	0.60	1.51
	Hail	-0.61	-0.28	0.14	3.43
	Drops	0.71	0.82	1.02	1.06
	Drops/Graupel	0.00	0.42	1.25	1.75
ρ_{hv}	Wet Graupel	0.93	0.95	0.98	1.00
	Dry Graupel	0.92	0.98	0.99	1.02
	Dry Snow	0.94	0.99	1.00	1.00
	Hail	0.94	0.95	0.98	1.00
	Drops	0.99	0.99	0.99	0.99
	Drops/Graupel	0.95	0.98	0.99	1.00

(Table 2 Continued on next page)

Table 2. Continued.

Radar Variable	Hydrometeor Type	X1	X2	X3	X4
K_{dp} (°/km)	Wet Graupel	-1.14	-0.08	0.13	0.78
	Dry Graupel	-1.14	-0.01	0.14	1.41
	Dry Snow	-0.09	0.00	0.12	0.48
	Hail	-0.88	0.00	0.88	2.65
	Drops	-0.20	-0.20	0.17	0.18
	Drops/Graupel	-2.32	0.00	0.36	0.87
LK_{dp}	Wet Graupel	-30.00	-30.00	-9.03	-1.09
	Dry Graupel	-30.00	-30.00	-8.40	1.50
	Dry Snow	-30.00	-30.00	-9.30	-3.18
	Hail	-30.00	-30.00	-0.54	4.23
	Drops	-30.00	-30.00	-7.79	-7.47
	Drops/Graupel	-30.00	-24.75	-4.46	-0.61

5.2.1 Graupel

This sub-section gives a broad comparison of graupel signatures that qualitatively combines the data from the wet and dry categories from the present study to match the graupel category in P09. With respect to reflectivity, Z_h, the middle and upper limits of the membership functions from Table 2 and A1 appear to be in fairly good agreement. The lower end of the membership function, though, is ~10 dB lower in Table 2 than in Table A1. These lower values may be quite reasonable for low-density, rimed aggregates that could produce 2D-C images classified as graupel.

Though Z_{dr} values from Table 2 do not differ markedly from the values presented in Table A2, the issue of possible Z_{dr} calibration differences between the radars needs to be resolved. These data should be used with caution and only after more data can be assimilated can any useful comparisons be made.

5.2.2 Dry snow

Differences seen when comparing the reflectivity values in Tables 2 and A1 can be accounted for by the fact that the T-28 observations were limited to convective-storm interiors where values toward the higher end of the reflectivity range for snow may be more common. The minimum values of Z_{dr} for snow are very similar in this study and in P09, but the differences become much greater for the X2, X3, and X4 points. Because dry snow was commonly observed in the present study, the upper echelon of these values may represent a preferred range in Z_{dr} space for convectively produced dry snow. Because of these observations, an operational membership function for dry snow should probably have a larger range of Z_{dr} values than given by P09, with higher values being represented.

The dry snow values for ρ_{hv} in Table 2 are nearly identical to those in Table A1, except for the X1 value. But again, this may be attributed to NBF skewing the X1 points to lower values. Otherwise there is good agreement between the ranges of ρ_{hv} values for dry snow found in this study and in that of P09.

The range of LK_{dp} values found in the present study (Table 2) is much narrower than that noted for dry snow by P09 (Table A1). While the present sample is limited, this could indicate potential difficulty in identifying dry-snow regions in convective storms using LK_{dp}.

5.2.3 Drops

The drops category included in this study covers a broad spectrum of the hydrometeor categories from that of P09 including big drops (BD), rain (RA), and heavy rain (HR). The present data should be viewed with caution; radar pixels entirely dominated by water drops were not found in this study, and the aircraft was rarely below the melting layer. Other studies, using data found in rain below the melting layer, may be better suited for determining the polarimetric variables of this type of precipitation. The spectrum of values of the polarimetric variables for samples classified as drops in this study falls within the P09 X2 and X3 points as seen in the respective sections of Table A1. These values appear quite representative of typical drops, but due to the small sample size and limited flight altitude range, the values found in this study do not show as much variation as indicated in Table A1.

5.2.4 Drops/graupel

This category best relates to the rain/hail (RH) category of P09. As noted previously, the graupel category involves many types of frozen hydrometeors, including some hailstones. Table A1 shows a range of Z_h values from 45-80 dBZ within the RH category, while Table 2 shows lower values between 27 and 46 dBZ—a large discrepancy. The absence of higher values is easily explained by the fact that the T-28 was directed during operations to avoid reflectivities greater than 55 dBZ to circumvent the most dangerous sections of a storm; consequently the KOUN samples on which Table 2 and

Fig. 2 are based included no sizable hail. The discrepancy in the smaller values may be due to the classification nomenclature. During image classification for this study, drops often were seen to exist side by side with true graupel and rimed aggregates; thus a smaller reflectivity range could well be expected for rain mixed with graupel compared to rain mixed with hail. The P09 scheme has no hydrometeor class that would be applicable to rain mixed with frozen aggregates or graupel, a phenomenon observed by the T-28 and one that may be quite common in convective storms. Because of these findings, it is suggested that a category for drops/graupel may need to be added to the current classifications within the automated HCAs.

5.2.5 Hail

Though this category in the T-28 data is strictly called hail, it was often observed mixed with liquid precipitation and thus will also be compared with the RH category of P09. Table 2 shows the minimum value Z_h for hail to be 40.5 dBZ while Table A1 shows an X1 value of 45 dBZ. Thus, these data suggest that the minimum value of Z_h for rain/hail in P09 may need to be lowered. The Z_{dr} value for X1 in Table 2 is slightly less than the value in Table A2. This illustrates that hail (or rain/hail mixtures) may have a propensity to exhibit larger negative Z_{dr} values than are reflected in the membership functions of P09. However, the radar calibration issue may preclude any definitive conclusions.

6. SUMMARY

The sensitivity of polarimetric radar to composition, size, shape, orientation, and distribution of hydrometeors can be exploited to make inferences about hydrometeor type by employing hydrometeor classification algorithms (HCAs) that utilize known ranges of polarimetric variables for the differing hydrometeor types. The purpose of this study is to help understand and improve upon the known ranges of polarimetric variables for differing hydrometeor types, as observed in or near the interior of mature convective storms.

Two types of polarimetric radars were used in this study: one with simultaneous transmission/reception of the orthogonal EM waves and one with alternating transmission of the orthogonal EM waves. Radar and *in situ* data were collected to represent a variety of hydrometeor types and phases. Methods were then developed to compare the polarimetric radar data to the *in situ* measurements. Hydrometeors in convective clouds, when above the melting layers, often exist in multiple phases and modes; that is, there is typically a mixture of hydrometeor types within a given portion of a storm. The propensity of hydrometeors to exist in mixed phases leads to many problems when it comes to hydrometeor identification with radar. For example, although one type of hydrometeor may dominate the precipitation mass—proportional to the 3rd power of the particle diameter—within a radar volume, because reflectivity is proportional to the diameter to the 6th power, a differing hydrometeor type may dominate the radar signature. Thus the present results offer useful insight into the hydrometeor identification problem.

Polarimetric radar variable ranges were found for each of six differing observed hydrometeor classifications: wet graupel, dry graupel, dry snow, drops, drops/graupel, and hail. “Membership functions” were then created using the *in situ* data gathered for this study and compared to the membership functions of the P09 HCA. The results presented here are generally consistent with the membership functions of the P09 HCA for many of the hydrometeor types identified, though some disparities were found. The disparities were then highlighted to show where, using the data collected from the T-28 observations, the membership functions of the operational HCA could be improved. It was found that the most improvement could be had in the graupel and dry snow categories. It was also suggested that an operational HCA should include another category for mixed-phase hydrometeors such as drops mixed with graupel or rimed aggregates. This type of mixture was found often in this study but is not addressed in the operational HCA. The only ‘mixed-phase’ category is for RH; while needed, it does not adequately represent all forms of mixed-phase hydrometeors.

This study also suggests that still more data are needed to fully address uncertainties in the membership functions of existing HCAs. Although the sample size here was limited, it was large enough to imply that this type of analysis may be useful in improving membership functions for fuzzy-logic-type HCAs. Future, similar studies with other armored aircraft that have the ability to make penetrations within convective or stratus type precipitation could prove most fruitful. Additional data obtained from below the melting layer will also augment the results of this study. As a final note, this study illustrated the complicated distribution of hydrometeor types within convective clouds. Because of this, making rigid hydrometeor class distinctions for such in-storm environments can be somewhat misleading.

Acknowledgements. This study was completed as part of a M.S. thesis at the South Dakota School of Mines and Technology and was supported in part by the Orville and Hjermstad Fellowships. The authors wish to thank Terry Schuur, Dusan Zrnić, Alexander Ryzhkov, Matthew Kumjian, and Scott Giangrande for their support with coding and the KOUN data retrieval. We are also grateful to Pat Kennedy who helped in obtaining useful CSU-CHILL data. Additionally, the comments by Roger Johnson were most appreciated.

REFERENCES

Aydin, K., T.A. Seliga, V. Balaji, 1986: Remote sensing of hail with a dual linear polarization radar. *J. Climate Appl. Meteor.,* **25,** 1475-1484.

Balakrishnan, N., and D.S. Zrnić, 1990: Estimation of rain and hail rates in mixed-phase precipitation. *J. Atmos. Sci.*, **47**, 565-583.

Beard, K.V., and C. Chuang, 1987: A new model for the equilibrium shape of raindrops. *J. Atmos. Sci.*, **44,** 1509-1524.

Bringi, V.N., and V. Chandrasekar, 2001: *Polarimetric Doppler Weather Radar: Principles and Applications.* Cambridge University Press, 636 pp.

Bringi, V.N., T.A. Seliga, K. Aydin, 1984: Hail detection with a differential reflectivity radar. *Science,* **225,** 1145-1147.

Bringi, V.N., R.M. Rasmussen, and J. Vivekanandan, 1986a: Multiparameter radar measurements in Colorado convective storms, Part I: Graupel melting studies. *J. Atmos. Sci.,* **43,** 2545-2563.

Bringi, V.N., J. Vivekanandan, and J.D. Tuttle, 1986b: Multiparameter radar measurements in Colorado convective storms, Part II: Hail detection studies. *J. Atmos. Sci.,* **43,** 2564-2577.

Clabo, D.R., 2009: Polarimetric Radar Signatures of Hydrometeors Observed within Mature Convective Storms. Masters Thesis. Department of Atmospheric Sciences, South Dakota School of Mines and Technology, 82 pp.

Doviak, R.J., and D.S. Zrnić, 1993: *Doppler Radar and Weather Observations.* Academic Press, 562 pp.

Doviak, R.J., V. Bringi, A. Ryzhkov, A. Zahrai, and D.S. Zrnić, 2000: Considerations of polarimetric upgrades of operational WSR-88D radars. *J. Atmos. Oceanic Technol.*, **17**, 257-278.

Doviak, R.J., J. Carter, V. Melnikov, D.S. Zrnić, 2002: Modifications to the research WSR-88D to obtain polarimetric data. Report of the National Severe Storms Laboratory. 51 p.

Feind, R.E., 2006: Thunderstorm in situ measurements from the armored T-28 aricraft: Comparison of measurements from two liquid water instruments and classification of 2D probe hydrometeor images. Ph.D. Dissertation. Atmospheric, Environmental, and Water Resources, South Dakota School of Mines and Technology, 102 pp.

Hall, M.P. M, J.W. Goddard and S.M. Cherry, 1984: Identification of hydrometeors and other targets by dual-polarization radar. *Radio Sci.,* **19,** 132-140.

Jameson, A.R., 1987: Relations among linear and circular polarization parameters measured in canted hydrometeors. *J. Atmos. Oceanic Tech.,* **4,** 634-646.

Knight, C.A., and N.C. Knight, 1970: The falling behavior of hailstones. *J. Atmos. Sci.,* **27,** 672-681.

Knight, C.A., and N.C. Knight, 1972: Conical Graupel. *J. Atmos. Sci.,* **30,** 118-124.

Kumjian, M.R., and A.V. Ryzhkov, 2009: Storm-Relative Helicity from Polarimetric Radar Measurements. *J. Atmos. Sci.,* **66,** 667-685.

Lesins, G.B., and R. List, 1986: Sponginess and drop shedding of gyrating hailstones in a pressure-controlled icing wind tunnel. *J. Atmos. Sci.,* **43,** 2813-2825.

Lim, S., V. Chandrasekar, and V.N. Bringi, 2005: Hydrometeor classification system using dual-polarization radar measurements: model improvements and in situ verification. *IEEE Trans. Geosci. Rem. Sens.*, **43**, 792-801.

Liu, H., and V. Chandrasekar, 2000: Classification of hydrometeors based on polarimetric measurements: Development of fuzzy logic and neuron-fuzzy systems, and in situ verification. *J. Atmos. Oceanic Technol.*, **17**, 140-164.

Park, H., A.V. Ryzhkov, D.S. Zrnić, and K. Kim, 2009: The hydrometeor classfication algorithm for the polarimetric WSR-88D: Description and application to an MCS. *Wea. Forecasting. (In press.)*

Ryzhkov, A.V., 2007: The impact of beam broadening on the quality of radar polarimetric data. *J. Atmos. Oceanic Tech.,* **24.**, 729-744.

Ryzhkov, A.V., and D.S. Zrnić: 2007: Depolarization in ice crystals and its effect on radar polarimetric measurements. *J. Atmos. Oceanic Tech.,* **24**, 1256-1267.

Ryzhkov, A.V., D.S. Zrnić, B.A. Gordon, 1998: Polarimetric method for ice water determination. *J. Appl. Meteor.,* **37,** 125-134.

Ryzhkov, A.V., T.J. Schuur, D.W. Burgess, P.L. Heinselman, S. Giangrande, and D.S. Zrnić, 2005: The Joint Polarization Experiment: Polarimetric rainfall measurements and hydrometeor classification, *Bull. Amer. Meteor. Soc.*, **86**, 809-824.

Seliga, T.A., and V.N. Bringi, 1976: Potential use of radar differential reflectivity measurements at orthogonal polarizations for measuring precipitation. *J. Appl. Meteor.*, **15**, 69-76.

Straka, J.M., and D.S. Zrnić, 1993: An algorithm to deduce hydrometeor types and contents from multiparameter radar data. *Preprints, 26th Int. Conf. on Radar Meteorology,* Norman, OK, Amer. Meteor. Soc., 513-516.

Straka, J.M., D.S. Zrnić, and A.V. Ryzhkov, 2000: Bulk hydrometeor classification and quantification using polarimetric radar data: Synthesis of relations. *J. Appl. Meteor.*, **39**, 1341-1372.

Vivekandan, J., V.N. Bringi, and R. Raghavan, 1990: Multiparameter radar modeling and observations of melting ice. *J. Atmos. Sci.,* **47**, 549-565.

Wallace J.M., and P.V. Hobbs, 1977: *Atmospheric Physics: An Introductory Survey.* Academic Press. 467 pp.

Zrnić, D.S., A.V. Ryzhkov, J. Straka, Y. Liu, and J. Vivekanandan, 2001: Testing a procedure for the automatic classification of hydrometeor types. *J. Atmos. Oceanic Technol.*, **18**, 892-913.

Appendix

Table A1. Membership function break points from Park *et al*. (2009).

P(Z(dBZ))

	GC/AP	BS	DS	WS	CR	GR	BD	RA	HR	RH
x1	15	5	5	25	0	25	20	5	40	45
x2	20	10	10	30	5	35	25	10	45	50
x3	70	20	35	40	20	50	45	45	55	75
x4	80	30	40	50	25	55	50	50	60	80

P(Z_{DR}(dB))

	GC/AP	BS	DS	WS	CR	GR	BD	RA	HR	RH
x1	-4	0	-0.3	0.5	0.1	-0.3	f2-0.3	f1-0.3	f1-0.3	-0.3
x2	-2	2	0.0	1.0	0.4	0.0	f2	f1	f1	0.0
x3	1	10	0.3	2.0	3.0	f1	f3	f2	f2	f1
x4	2	12	0.6	3.0	3.3	f1+0.3	f3+1.0	f2+0.5	f2+0.5	f1+0.5

P(ρ_{hv})

	GC/AP	BS	DS	WS	CR	GR	BD	RA	HR	RH
x1	0.5	0.3	0.95	0.88	0.95	0.90	0.92	0.95	0.92	0.85
x2	0.6	0.5	0.98	0.92	0.98	0.97	0.95	0.97	0.95	0.90
x3	0.9	0.8	1.00	0.95	1.00	1.00	1.00	1.00	1.00	1.00
x4	0.95	0.83	1.01	0.985	1.01	1.01	1.01	1.01	1.01	1.01

P(LK_{dp})

	GC/AP	BS	DS	WS	CR	GR	BD	RA	HR	RH
x1	-30	-30	-30	-30	-5	-30	g1-1	g1-1	g1-1	-10
x2	-25	-25	-25	-25	0	-25	g1	g1	g1	-4
x3	10	10	10	10	10	10	g2	g2	g2	g1
x4	20	10	20	20	15	20	g2+1	g2+1	g2+1	g1+1

P(SD(Z)(dB))

	GC/AP	BS	DS	WS	CR	GR	BD	RA	HR	RH
x1	2	1	0	0	0	0	0	0	0	0
x2	4	2	0.5	0.5	0.5	0.5	0.5	0.5	0.5	0.5
x3	10	4	3	3	3	3	3	3	3	3
x4	15	7	6	6	6	6	6	6	6	6

P(SD(Φ_{DP})(deg))

	GC/AP	BS	DS	WS	CR	GR	BD	RA	HR	RH
x1	30	8	0	0	0	0	0	0	0	0
x2	40	10	1	1	1	1	1	1	1	1
x3	50	40	15	15	15	15	15	15	15	15
x4	60	60	30	30	30	30	30	30	30	30

Table A2. Calculated values for Z_{dr} and LK_{dp} membership functions using equations and values found in Park *et al*. (2009). Use in conjunction with Table A1.

P(Z_{dr})(dB)

	GR	BD	RA	HR	RH
X1	-0.3	0.6	-0.8	0.5	-0.3
X2	0.0	1.3	-0.4	1.1	0.0
X3	1.5	5.4	4.4	6.9	3.9
X4	2.2	7.0	6.1	8.8	5.0

P(LK_{dp})(dB)

	GR	BD	RA	HR	RH
X1	-30	-29	-29	-29	-10
X2	-25	-24	-24	-24	-4.0
X3	10	0.50	0.50	0.50	16
X4	20	4.0	4.0	4.0	21